Carbohydrate Polymers 103 (2014) 22–31

Contents lists available at ScienceDirect

Carbohydrate Polymers

journal homepage: www.elsevier.com/locate/carbpol

Effect of silver nanoparticles and cellulose nanocrystals on electrospun poly(lactic) acid mats: Morphology, thermal properties and mechanical behavior

Ilaria Cacciotti [a,*], Elena Fortunati [b], Debora Puglia [b], Josè Maria Kenny [b,c], Francesca Nanni [a]

[a] University of Rome "Tor Vergata", Department of Industrial Engineering, INSTM RU "Tor Vergata", Via del Politecnico 1, 00133 Rome, Italy
[b] Materials Engineering Centre, UdR INSTM, NIPLAB, University of Perugia, Strada di Pentima 4, 05100 Terni, Italy
[c] Institute of Polymer Science and Technology, CSIC, Madrid, Spain

ARTICLE INFO

Article history:
Received 2 September 2013
Received in revised form 4 November 2013
Accepted 27 November 2013
Available online 4 December 2013

Keywords:
Electrospinning
Poly(lactic acid)
Cellulose nanocrystals
Silver nanoparticles
Self-assembling
Honeycomb structure

ABSTRACT

The fabrication of ternary fibrous mats based on poly(lactic) acid (PLA), cellulose nanocrystals (CNCs, both pristine (p-CNCs) and modified with a commercial surfactant (s-CNCs)) and silver (Ag) nanoparticles by electrospinning is reported. Amounts of 1 and 5 wt.% were selected for Ag and CNCs, respectively. Neat PLA and binary PLA/Ag, PLA/p-CNCs and PLA/s-CNCs were produced as references.

The CNCs and Ag influence on the microstructural, thermal and mechanical properties was investigated. The Ag and/or p-CNCs addition did not remarkably affect fiber morphology and average size dimension (between (468 ± 111) and (551 ± 122) nm), whereas the s-CNCs presence led to the deposition of a honeycomb-like network on a underneath layer of randomly oriented fibers. The efficiency of the surfactant use in promoting the CNC dispersion was demonstrated. A slight enhancement (e.g. around 25%, in terms of strength) of the mechanical properties of p-CNCs loaded fibers, particularly for PLA/Ag/p-CNCs, was revealed, whereas mats with s-CNCs showed a decrement (e.g. around 35–45%, in terms of strength), mainly imputable to the delamination between the upper honeycomb-like layer and the lower conventional fibrous mat.

1. Introduction

Electrospinning consists in a cheap and user friendly technique to fabricate polymeric, ceramic and composite fibrous membranes, with diameters ranging from hundreds to tens of nanometers (Frenot & Chronakis, 2003) and could be integrated with conventional techniques to create innovative multifunctional patterned micro/nano-structures, starting from different materials. Electrospun membranes are considered promising and excellent candidates for applications in filtration, food texture alterations, encapsulation of food additives, active and bioactive packaging elements, separation membranes, reinforcement in composite materials (Bianco, Di Federico, & Cacciotti, 2011; Lamastra et al., 2012), intelligent, functional and active packaging sectors for food and pharmaceuticals (Kriegel, Arrechi, Kit, McClements, & Weiss, 2008; Lagaron & Lopez-Rubio, 2011; Sanchez-Garcia, Lopez-Rubio, & Lagaron, 2010; Weiss, Takhistov, & McClements, 2006). In particular, food industry could employ electrospun fibers in several ways: as a building/reinforcement element of composite green food packaging material, as building elements of the food matrix for imitation/artificial foods, as nanostructured and microstructured scaffolding for bacterial cultures, as edible carriers for encapsulation of food additives or to modify food properties and in the design of novel active and bioactive packaging technologies (Lagaron & Lopez-Rubio, 2011).

Electrospun fibers provide additional advantages compared to film and sheet carriers due to their nano- or submicron-scale diameter and consequent very large surface area, and, thus, are ideal as sensors (Arecchi, Scampicchio, Drusch, & Mannino, 2010), for biomolecules and enzymes immobilization, controlled release (Jiang et al., 2005) and filtration (Ramakrishna et al., 2010).

Several polymers have been employed to prepare electrospun fibers and among them PLA is receiving a lot of attention, since it is a renewable resources derived thermoplastic polyester, commercially available and widely used in packaging industry, due to its high transparency, stiffness and thermoformability (Siracusa, Rocculi, Romani, & Dalla Rosa, 2008). Moreover it is not only biodegradable, but also compostable and thus its employment is strongly desirable, in order to minimize the environmental impact

* Corresponding author. Tel.: +39 0672594482; fax: +39 0672594328.
E-mail address: ilaria.cacciotti@uniroma2.it (I. Cacciotti).

0144-8617/$ – see front matter © 2013 Elsevier Ltd. All rights reserved.
http://dx.doi.org/10.1016/j.carbpol.2013.11.052

of petroleum based plastics (Petersen, Nielsen, & Olsen, 2001) as well as the environmental concerns raising from waste management (Lagaron & Lopez-Rubio, 2011). Plastic recycling, in fact, is not often economically viable, especially in the case of food packaging due to the contamination of food (Kijchavengkul, Auras, Rubino, Ngouajio, & Fernandez, 2006). However compostable polymers still present a lot of drawbacks with respect to the conventional petroleum-based polymers used in packaging applications, such as inherent brittleness, low impact resistance, fair thermal properties, toughness, water vapour and gas barrier properties. Thus, in order to improve some of these properties, several kinds of fillers have been recently proposed, including natural and synthetic cellulose fibers (Fortunati, Puglia, Santulli, Sarasini, & Kenny, 2012), regenerated cellulose fibers (Lim, Son, Lee, Park, & Cho, 2001), wood fibers (Huda, Drzal, Misra, & Mohanty, 2006), recycled newspaper fibers (Huda, Drzal, Mohanty, & Misra, 2007), plant fibers from kenaf (Ochi, 2008), and microfibrillated cellulose (MFC) (Galina Rodionova, Lenes, Eriksen, & Gregersen, 2011).

Cellulose nanocrystals (CNCs) have been widely used as reinforcement fillers, since they present good mechanical properties, are biodegradable and biocompatible and present low density. However, they are difficult to process, since they tend to agglomerate and show low thermal stability; thus it is very challenging to obtain good CNCs dispersion and to preserve their properties in polymeric matrices by means of common processing techniques, such as extrusion and melt spinning processes (Oksman, Mathew, Bondeson, & Kvien, 2006). To overcome these drawbacks, electrospinning was used in this work, since it takes place at ambient conditions and it has been already proven to be particularly suitable for encapsulating thermally labile molecules and/or low temperature degradable fillers (i.e. cellulose nanocrystals) (Qi, Hu, Xu, & Wang, 2006).

In order to promote stability in the dispersion of the CNCs, their surface was modified using a surfactant that, on the basis of previous papers (Bondeson & Oksman, 2007; Bondeson, Mathew, & Oksman, 2006; Fortunati, Armentano, Zhou, Puglia, et al., 2012; Fortunati, Armentano, Zhou, Iannoni, et al., 2012; Heux, Chauve, & Bonini, 2000; Oksman et al., 2006), was an acid phosphate ester of ethoxylated nonylphenol.

In the present paper the production and characterization of multifunctional ternary poly(lactic acid) (PLA) fibers, loaded with cellulose nanocrystals (CNCs, both pristine and modified with a surfactant) and silver nanoparticles, by electrospinning technique is reported for the first time. Silver nanoparticles were added since they showed good conductivity, chemical stability, catalytic activity and, mainly, inherent antimicrobial properties that make them appealing for applications in biomedical and food packaging sectors.

In previous reports (Shi et al., 2012; Xiang, Joo, & Frey, 2009), only binary fibrous systems composed of PLA and pristine CNCs have been investigated and the use of the modified CNCs as fillers in electrospun PLA fibers has not been considered yet.

The main purpose of this work was to investigate the influence of the co-presence of the cellulose nanocrystal and silver nanoparticle fillers on the morphological, thermal and mechanical properties of the produced fibrous mats, reporting the neat PLA and binary systems as references.

2. Materials and methods

2.1. Materials

Poly(lactic) acid (PLA 3051D, specific gravity of 1.25 g/cm^3, molecular weight (M_n) of *ca.* 1.42×10^4 g/mol) was supplied by *Nature Works*®, USA. Commercial silver nanopowder (Ag, P203, size distribution range 20–80 nm) was purchased by *Cima NanoTech*®, USA.

Microcrystalline cellulose (MCC, dimensions of 10–15 mm) was supplied by *Sigma–Aldrich*, Italy.

2.2. Synthesis of pristine and modified cellulose nanocrystals

Cellulose nanocrystal (p-CNCs) suspension was prepared from microcrystalline cellulose by sulphuric acid hydrolysis following the recipe used by Cranston and Gray (2006). Hydrolysis was carried out with 64% (w/w) sulphuric acid at 45 °C for 30 min with vigorous stirring. After removing the acid, dialysis, and ultrasonic treatment were performed. The resultant cellulose nanocrystal aqueous suspension was approximately 0.5% (w/w) by weight and the yield was *ca.* 20%. The obtained pristine cellulose crystals showed the typical acicular structure with the dimensions ranging from 100 to 200 nm in length and 5–10 nm in width as previously reported (Fortunati, Armentano, Zhou, Puglia, et al., 2012; Fortunati, Armentano, Zhou, Iannoni, et al., 2012).

Cellulose nanocrystals were modified with a surfactant, an acid phosphate ester of ethoxylated nonylphenol, in order to increase the dispersion in the polymer matrix and to enhance the final properties of nanocomposite porous systems. The CNCs modified with surfactant (designed as s-CNCs) were prepared by adding the Beycostat A B09 (CECCA S.A.) (Heux et al., 2000) to the suspension containing nanocrystals, in portion of 4/1 (w/w), using the weight of p-CNCs estimated at the end of the hydrolysis process. This high content of surfactant is necessary to re-disperse the cellulose nanostructures in organic solvent after the freeze-drying process. The pH of the suspension was then adjusted to 8.5 using the same 0.25 wt.% NaOH solution as above.

2.3. Preparation of PLA based suspensions

2.3.1. PLA/Ag binary suspensions

The Ag nanoparticles disagglomeration was performed in chloroform ($CHCl_3$, 99%, *Carlo Erba Reagents*) by sonication for 1 h in an ice bath. Successively, proper amounts of PLA pellets and of N,N-dimethylformamide (DMF, $(CH_3)_2NOCH$, 99.8%, *Carlo Erba Reagents*) were added to the Ag nanoparticle suspensions in order to obtain the desiderated amounts (i.e. PLA concentration of 15% (w/v) with respect to the solvents, solvent mixture $CHCl_3$:DMF in a volume ratio 67:33, Ag nanoparticles amount of 1 wt.% with respect to the polymer, Table 1).

Finally, the obtained hybrid suspension was magnetically stirred at around 40–50 °C for 2–3 h and then at room temperature for 12–24 h, in order to promote the complete dissolution of the polymer.

The Ag content (i.e. 1 wt.%) was properly selected on the basis of previous reports (Fortunati, Armentano, Zhou, Puglia, et al., 2012; Fortunati, Armentano, Zhou, Iannoni, et al., 2012).

2.3.2. PLA/CNCs binary suspensions

In order to obtain an effective dispersion of the pristine and modified CNCs, a proper amount of the freeze-dried CNCs was suspended in N,N-dimethylformamide (DMF, $(CH_3)_2NOCH$, 99.8%, *Carlo Erba reagents*) and ultrasonicated (*Sonics Vibracell CV33*) for 2 min at 40% amplitude in an ice bath. Afterwards proper amounts of PLA pellets and of chloroform were added to the CNCs suspension in order to obtain the desiderated composition (i.e. PLA concentration of 15% (w/v) with respect to the solvents, solvent mixture $CHCl_3$:DMF in a volume ratio 67:33, CNCs amount of 5 wt.% with respect to the polymer, Table 1).

Table 1
Designation, composition and average fiber diameter of neat and hybrid PLA based electrospun mats, and viscosity and conductivity values of the related solutions and suspensions.

Sample	%wt.				Viscosity (cP)	Conductivity (μS/cm)	Average fiber diameter (nm)
	[PLA]	[Ag]	[p-CNCs]	[s-CNCs]			
$CHCl_3$	–	–	–	–	0.25 ± 0.01	0.007 ± 0.004	–
DMF	–	–	–	–	0.25 ± 0.01	1.625 ± 0.014	–
$CHCl_3$:DMF, 67:33	–	–	–	–	0.25 ± 0.01	1.848 ± 0.015	–
PLA					163.00 ± 0.07	0.930 ± 0.016	551 ± 122
PLA/Ag	99	1	–	–	155.00 ± 0.39	4.440 ± 0.025	468 ± 111
PLA/p-CNCs	95	–	5	–	280.00 ± 2.36	5.550 ± 0.013	479 ± 121
PLA/s-CNCs	95	–	–	5	214.00 ± 0.37	3.279 ± 0.027	521 ± 116
PLA/Ag/p-CNCs	94	1	5	–	299.00 ± 1.30	5.890 ± 0.0180	521 ± 107
PLA/Ag/s-CNCs	94	1	–	5	250.00 ± 0.35	3.303 ± 0.051	467 ± 113

The CNCs content (i.e. 5 wt.%) was chosen on the ground of previous results (Fortunati, Armentano, Zhou, Puglia, et al., 2012; Fortunati, Armentano, Zhou, Iannoni, et al., 2012).

2.3.3. PLA/Ag/CNCs ternary suspensions

In the case of ternary systems, proper aliquots of CNCs (p-CNCs or s-CNCs) and of Ag suspensions were mixed and a suitable amount of PLA (15%, wt/v in $CHCl_3$:DMF 67:33) was added in order to obtain the compositions reported in Table 1.

The obtained mixture was magnetically stirred at around 40–50 °C for 2 h and then at room temperature for 12–24 h, up to complete polymer dissolution.

2.4. Fabrication of neat and hybrid PLA based mats by electrospinning

The prepared hybrid suspensions were poured in a glass syringe (*Socorex*, *Switzerland*) equipped with a 18 G needle, fixed in a digitally controlled syringe pump (*KD Scientific*, *MA*, *USA*) and electrospun in air at room temperature in the following conditions: applied voltage 16 kV (*Spellman*, *Model SL 30*, *NY*, *USA*), feed rate 0.5 ml/h, needle-target distance 15 cm.

After deposition, membranes were detached from the target by ethanol (EtOH) immersion, dried under vacuum and stored in air drier. As a reference sample, neat PLA mat was also produced employing the same experimental procedure. In Table 1 the samples designation and the related compositions are summarized.

2.5. Characterization techniques

2.5.1. Viscosity and conductivity of polymeric solutions and suspensions

The viscosity of all polymeric solutions/suspensions was measured at 25 °C by means of a digital viscosimeter (*Brookfield DV-II+*, *Middleboro*, *MA*, *USA*) equipped with a SC4-21 spindle, at 20 rpm. Electrical conductivities were registered at 25 °C by means of an electrical conductimeter (CDM230, *Analitica De Mori*, *Italy*) calibrated with a 0.01 D KCl solution (standard conductivity value of 1.408 mS/cm). In both cases five measurements were acquired, at least, for each solution/suspension, in order to provide an average value.

2.5.2. Morphology of PLA based mats

The morphology of the electrospun mats was investigated by means of scanning electron microscopy (SEM) (*Cambridge Stereoscan 300*, *Leo Supra 35*).

Energy dispersive spectroscopy (EDS) mapping of Ag element was carried out on 24.3 μm × 18.2 μm areas by means of *INCA Energy 300*, *Oxford ELXII detector*, in order to evaluate its distribution within the fibrous mats. The average fiber diameter was determined considering around 50 randomly selected fibers from SEM micrographs (*ImageJ*, NIH).

2.5.3. Thermal properties of PLA based mats

Differential scanning calorimetry (DSC, *Mettler Toledo 822e/400*) measurements were performed in the following conditions: sample weight ~5 mg, nitrogen atmosphere, range temperature from 25 °C to 250 °C, heating and cooling rates of 10 °C/min. Two heating and one cooling scans were carried out. Melting temperatures ($T_{m\mathrm{I}}$ and $T_{m\mathrm{II}}$), cold crystallization temperatures ($T_{cc\mathrm{I}}$ and $T_{cc\mathrm{II}}$), melting enthalpies ($\Delta H_{m\mathrm{I}}$ and $\Delta H_{m\mathrm{II}}$), cold crystallization enthalpies ($\Delta H_{cc\mathrm{I}}$ and $\Delta H_{cc\mathrm{II}}$), and crystallinity degrees (χ_{I} and χ_{II}) were evaluated in the first and in the second heating scans.

The crystallinity degree (χ) was calculated as:

$$\chi = \frac{\Delta H_m - \Delta H_{cc}}{\Delta H_{0,m}(1 - m_f)} \times 100 \quad (1)$$

where ΔH_m, $\Delta H_{0,m}$ and ΔH_{cc} represent scan-related enthalpy, melting enthalpy for 100% crystalline PLA material (i.e. 93 J/g (Riga, Zhang, & Collis, 2004)) and cold crystallization enthalpy, respectively; m_f is the weight fraction of the filler within the nanohybrid fibers (Sarasua, López Arraiza, Balerdi, & Maiza, 2005).

2.5.4. Mechanical properties of PLA based electrospun mats

Uniaxial tensile tests were performed on dog-bone specimens (width 4.8 mm, length 22.25 mm), at 1.2 mm/min to rupture by an electromechanical machine equipped with a 100 N load cell (*Lloyd LRX*), following ASTM D1708 and ASTM D882 for elastic modulus calculation. Four specimens were considered for each electrospun matrix. The ultimate stress ($\sigma_{\max}$) was calculated considering the nominal cross-sectional area of the tensile specimen. All mechanical properties were calculated considering the nominal specimen cross-section. Finally, the fracture surface of electrospun samples was investigated by means of scanning electron microscopy (FE-SEM, *Cambridge Leo Supra 35*), aimed to investigate the morphological response of the fibers to the mechanical stress.

2.5.5. Dynamic mechanical thermal analysis of PLA based mats

Viscoelastic properties of the electrospun mats were investigated by means of the dynamic mechanical thermal analysis (DMTA) (*Tritec 2000 DMA*, *Triton Technology*, *UK*), in the tensile mode. The tests were carried out on rectangular specimens (15 mm × 3 mm) with thickness (0.40 ± 0.14) mm. Measurements were performed in the temperature range of 30–110 °C (5 °C/min heating ramp), applying a displacement of 0.02 mm at a frequency of 1 Hz. The obtained results were discussed in terms of storage modulus (E') and loss factor ($\tan\delta$), being representative of the viscoelastic damping of the polymer system.

Glass transition temperatures (T_g) were evaluated as temperatures corresponding to $\tan\delta$ maximum. At least four specimens were tested for each investigated mats.

3. Results and discussion

3.1. Properties of the PLA based solutions/suspensions

The viscosity and conductivity of the prepared solutions and suspensions are collected in Table 1.

As a reference, the values of the used solvents, i.e. $CHCl_3$, DMF and the $CHCl_3$:DMF mixture in a 2:1 volume ratio, are reported. As expected, the DMF presents a remarkably higher conductivity with respect to the $CHCl_3$ (i.e. 1.625 μS/cm vs. 0.065 μS/cm), and, thus, its use promotes the electrospinning process.

For the binary and ternary systems, the addition of the nanofiller(s) led to an increment of both viscosity and conductivity, in particular in the case of p-CNCs loaded ones. The ternary composites were characterized by slightly higher values with respect to the related binary ones, due to the Ag nanoparticles presence.

Moreover, it is worthy to note that in the case of s-CNCs containing suspensions, remarkably lower viscosity values were obtained with respect to the correspondent p-CNCs ones (214 cP vs. 280 cP and 250 cP vs. 299 cP, as average values, for the binary and ternary systems, respectively), ascribable to the surfactant presence.

3.2. Morphology and microstructure of PLA based mats

In Figs. 1 and 2 the morphologies of obtained neat and hybrid PLA based fibrous mats are compared and in Table 1 the values of the average diameter sizes are collected.

All the deposited mats were composed of smooth, randomly oriented, homogeneous, uniform and bead-free fibers. The presence of Ag and/or CNCs fillers favored the deposition of slightly thinner fibers compared to the neat PLA ones (i.e. (551 ± 122) nm), due to the higher conductivity of the hybrid suspension (Table 1), in agreement with the literature (Ramakrishna, Fujihara, Teo, Lim, & Ma, 2005).

In the case of PLA/Ag mat and, generally for all Ag loaded samples (i.e. PLA/Ag/p-CNCs and PLA/Ag/s-CNCs), the metallic filler was well dispersed throughout all the fibrous mats, as evidenced in the related Ag EDS map (Fig. 1b). However, some sporadic and random Ag nanoparticles clusters were detected within the fibers.

The addition of pristine p-CNCs to PLA suspension did not alter the fiber morphology and the presence of agglomerates was not evidenced, allowing to obtain submicrometric (average diameter (479 ± 121) nm) defect free fibers (Fig. 1a).

Similarly SEM micrographs of PLA/Ag/p-CNCs mats revealed homogenous and uniform fibers, with well dispersed Ag nanoparticles, accompanied by some Ag agglomerates (Fig. 1b).

Finally, both the binary and ternary systems containing surfactant modified s-CNCs were surprisingly composed of bundles of submicrometric (average diameter size 521 nm, Table 1) fibers organized in a honeycomb-like network, with cells formed by polygons with a random number of sides (Fig. 2). The honeycomb-like meshes were mainly composed of pentagons, and hexagons and were clearly separated by wall-like boundaries, constituted by self-aligning fibers, obtaining polygonal shape channels characterized by three-branched walls with the intersecting angle approaching 120°. The walls of the honeycomb network consisted in bundles of thick wet fibers which in turn favored the alignment and deposition of further fibers in a self-sustained process (Ahirwal, Hébraud, Kádár, Wilhelm, & Schlatter, 2013).

This experimental evidence is ascribable to the presence of the modified s-CNCs, with a possible self-assembling phenomenon that occurred after an initial deposition of randomly distributed fibers, comparable to that observed for the other samples (Fig. 2). It is worthy to highlight that this kind of structure has been never obtained

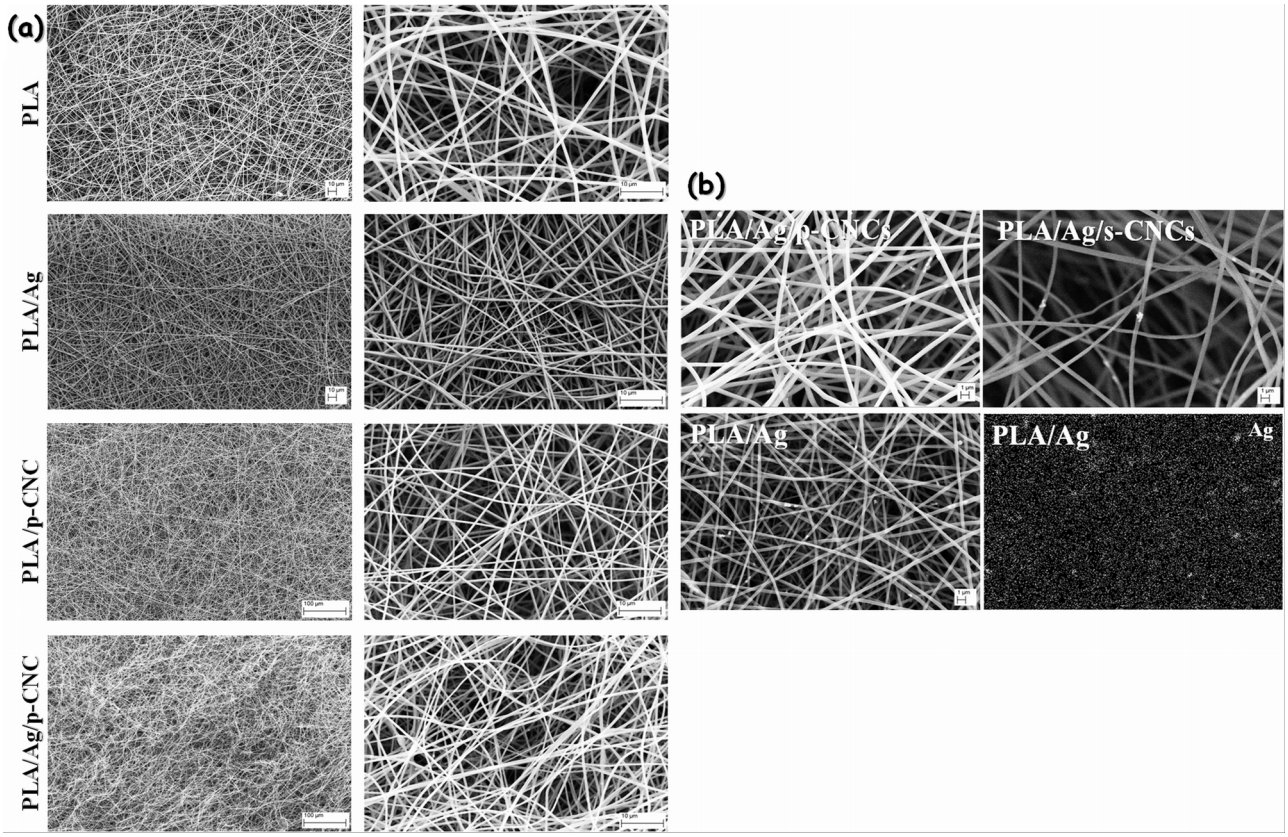

Fig. 1. (a) SEM micrographs of electrospun PLA, PLA/Ag, PLA/p-CNCs and PLA/Ag/p-CNCs mats and (b) SEM micrographs of electrospun PLA/Ag/p-CNCs, PLA/Ag/s-CNCs, PLA/Ag mats and related EDS Ag map.

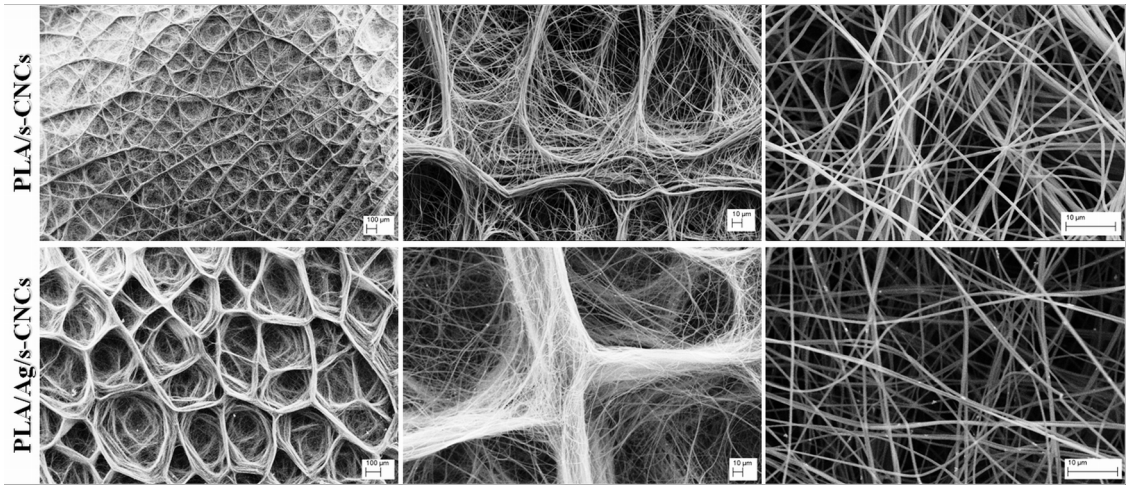

Fig. 2. SEM micrographs of electrospun PLA/s-CNCs and PLA/Ag/s-CNCs mats.

in the case of electrospun PLA fibers and present a wide range of possible applications, due to the peculiar shape, very similar to that observed in colloidal crystals and foams as a result of a self-similar pattern growth and to some natural organization, such as plant parenchyma.

This phenomenon was also observed by Deitzel, Kleinmeyer, Harris, and Tan (2001), Yan et al. (2011), Thandavamoorthy, Gopinath, and Ramkumar (2006) and Ahirwal et al. (2013) for the polyacrylonitrile, polyvinyl alcohol, polyethylene oxide, polyurethane and poly(ε-caprolactone).

They hypothesized that the formation of dimples or honeycomb structure can be associated to the presence of residual charges on the collected nanofibers leading to the occurring of a self-organization.

In particular, according to Yan et al. (2011), the formation of the honeycomb structure is ascribable to the competitive actions of two pivotal driving forces, i.e. the surface tension and electrostatic repulsion, reporting that wetter fibers tend to form more defined honeycomb structure while drier fibers tend to form randomly distributed fibers. In fact they stated that the surface tension promotes the wet fibers to stick together while the electrostatic repulsion pushes the fibers apart. It is likely that the incoming fibers tend to preferentially deposit on points of contact between fibers since these points feature a lower charge density compared to other parts of the fiber (Morozov & Vsevolodov, 2007), leading to the progressive building of a honeycomb structure.

Since the fiber deposition pattern is dominated by the fiber charge intensity and the repulsive forces exerted by the already deposited fibers, it is expected that the collected fibers tend to repel the incoming similarly charged fibers and drive them toward the nearby conducting points on the collector screen for easier charge dissipation.

Ahirwal et al. (2013) proposed a scheme of the temporal evolution in the self-assembly mechanism, reporting that during the first minutes of the electrospinning process, the electrospun jet is subjected to a homogeneous electric field that induces a pseudo-random deposition. It was hypothesized that the residually wet fibers are in very good contact with the collector, allowing efficient electric charge dissipation, whereas thin dry fibers tend to remain suspended in the air and retain their electric charge (Ahirwal et al., 2013).

Thus, as also underlined by Yan et al. (2011), a heterogeneous distribution of electric charges accumulates at the collector surface, leading to a perfect template that promotes the formation of the first honeycomb layer. Successively, it is expected that the thickness of the honeycomb patterns continuously increase with increasing electrospinning time (Ahirwal et al., 2013).

3.3. Thermal properties of PLA based mats

DSC analyses were carried out on neat and hybrid PLA based samples, in order to investigate the influence of the fillers on the thermal properties of the produced fibers. The glass transition (T_g), melting (T_m), cold crystallization (T_{cc}) temperatures, the melting (ΔH_m) and cold crystallization (ΔH_{cc}) enthalpies and the crystallinity degree (χ), related to the first and the second heating scans, are summarized in Table 2. The first and second heating scan DSC curves are compared in Fig. 3a and b, respectively.

From the comparison between the data reported in Table 2, related to the first heating scan, it is clear that filler addition did not seem to significantly influence the melting temperature (T_{mI}), whereas it led to an increment of around 3 °C of the glass transition temperature (T_{gI}, 60 °C for neat PLA vs. 63 °C for the hybrid systems). On the other hand, the cold crystallization temperature (T_{ccI}), presented a decrement of around 3–5 °C, particularly in the case of the nanocomposites containing the modified s-CNCs (94 °C for the neat PLA vs. 87–88 °C for PLA/s-CNCs and PLA/Ag/s-CNCs systems) (Table 2). This result suggests a good dispersion in the case of s-CNCs, since well-dispersed nanofillers are able to promote the cold crystallization at lower temperatures (Bianco, Di Federico, et al., 2011; Bianco, Bozzo, et al., 2011; Fortunati, Armentano, Zhou, Puglia, et al., 2012; Wu et al., 2007).

The p-CNCs were less efficient in favoring the crystallization, since they were more agglomerated with consequent smaller contact area between the fillers and the polymer matrix (Fortunati, Armentano, Zhou, Puglia, et al., 2012) (Table 2).

In addition, it is evident that, in the case of neat PLA the cold crystallization occurred in a wide temperature range (around 30 °C), whereas the filler addition led to a narrowing (around 20 °C) of this temperature range and to a more intense T_{ccI} peak, suggesting that the fillers were able to promote PLA nucleation during electrospinning process (Xiang et al., 2009).

Interestingly, the obtained T_{ccI} values were remarkably lower with respect to those registered for related solvent cast films (i.e. 122–110 °C) (Fortunati, Armentano, Zhou, Puglia, et al., 2012), due to the very large surface to volume ratio of the electrospun membranes (Zong et al., 2002) and probably to the presence of numerous crystal nuclei (Huang, Zhang, Kotaki, & Ramakrishna, 2003).

Furthermore, in the case of PLA/Ag and PLA/Ag/p-CNCs, two melting peaks were detected in the first heating scan DSC curves:

Table 2
Differential scanning calorimetry (DSC) data for the neat and hybrid PLA based fibrous mats.

	I Heating						
	T_{gI}(°C)	T_{ccI}(°C)	ΔH_{ccI}(J/g)	ΔH_{mI}(J/g)	T_{m1I}(°C)	T_{m2I}(°C)	χ_I(%)
PLA	60.3 ± 0.8	94.3 ± 0.5	20.7 ± 1.8	22.9 ± 2.4	–	147.9 ± 1.3	2.4 ± 1.4
PLA/Ag	63.5 ± 0.2	91.3 ± 0.7	15.4 ± 0.7	27.8 ± 0.6	145.0 ± 0.3	148.8 ± 0.3	13.1 ± 0.6
PLA/p-CNCs	63.1 ± 0.4	91.5 ± 0.4	12.8 ± 2.1	25.4 ± 1.7	–	149.0 ± 0.5	12.9 ± 1.4
PLA/s-CNCs	61.9 ± 0.9	87.3 ± 0.4	15.1 ± 1.5	27.3 ± 1.0	–	148.1 ± 0.3	12.4 ± 0.7
PLA/Ag/p-CNCs	60.0 ± 1.4	91.2 ± 0.4	11.5 ± 2.5	24.0 ± 3.7	146.1 ± 0.3	148.4 ± 0.2	12.7 ± 2.4
PLA/Ag/s-CNCs	62.8 ± 0.1	88.6 ± 0.2	16.2 ± 0.9	27.1 ± 0.6	–	149.1 ± 0.2	11.0 ± 0.3
	II Heating						
	T_{gII}(°C)	T_{ccII}(°C)	ΔH_{ccII}(J/g)	ΔH_{mII}(J/g)	T_{m1II}(°C)	T_{m2II}(°C)	χ_{II}(%)
PLA	59.0 ± 1.1	–	–	1.2 ± 0.6	–	147.1 ± 0.4	1.3 ± 0.7
PLA/Ag	59.1 ± 0.6	–	–	0.6 ± 0.3	–	147.5 ± 1.6	0.6 ± 0.3
PLA/p-CNCs	59.7 ± 0.5	–	–	1.2 ± 0.3	–	148.4 ± 0.1	1.4 ± 0.5
PLA/s-CNCs	52.7 ± 1.7	112.8 ± 5.3	28.2 ± 4.7	28.4 ± 3.7	144.3 ± 2.1	151.2 ± 0.3	–
PLA/Ag/p-CNCs	61.3 ± 1.8	–	–	3.1 ± 1.6	–	146.4 ± 2.3	3.1 ± 1.6
PLA/Ag/s-CNCs	55.6 ± 0.1	118.5 ± 1.5	23.7 ± 0.7	24.6 ± 0.2	147.2 ± 0.2	151.8 ± 0.4	0.9 ± 0.4

a first little shoulder (T_{m1I}), followed by the effective melting temperature (T_{m2I}). This experimental evidence suggested that the Ag nanoparticles and the pristine CNCs were able to promote the rearrangement of the PLA chains and the formation of heterogeneous crystalline phases in PLA during the thermal crystallization. The same phenomenon was revealed in the case of PLA/s-CNCs and PLA/Ag/s-CNCs in the second heating scan. In fact, the fillers addition usually promotes the formation of small crystals whose melting occurs at lower temperatures (He, Fan, Wie, & Li, 2006; Shi, Mou, Gao, Yang, & Guo, 2010; Sim & Han, 2010; Suksut & Deeprasertkul, 2011).

Regarding the crystallinity degrees, in general, in electrospun mats they are very low, indicating that the majority of the chains are in the amorphous state, due to the intrinsic features of the electrospinning process. In fact, the rapid evaporation of the solvent and the high elongation strain rate of the jet of the electrospinning usually lead to rapid solidification of stretched chains during the later stages of the process, hindering the development of crystallinity. Thus the stretched chains do not have enough time to organize into crystals before they are solidified (Zong et al., 2002).

In details, comparing the registered crystallinity degrees, higher values were obtained in the case of hybrid systems, acting the particles as crystallinity nuclei. In fact, higher melting enthalpies correspond to the formation of smaller and less dense crystals in the PLA matrix (Suksut & Deeprasertkul, 2011).

Concerning the second heating scan, the related DSC curves are shown in Fig. 3b. It is interesting to note that the glass transition is hardly detectable and the cold crystallization phenomenon was only identified in the s-CNCs loaded samples, indicating that, in these samples, the applied cooling conditions were not able to induce the complete PLA crystallization. This experimental evidence was a further confirmation of the surfactant influence, being able to interact with the polymer chains and affect its thermal properties and crystallization process.

In the second heating scan, the T_g further reduced in the case of s-CNCs based systems (Table 2), due to the better dispersion of the fillers within the fibrous mats with consequent development of a higher interphase fraction and to the surfactant influence.

The cold crystallization temperatures were higher than those registered during the first scan, revealing the different organization of the molecular chains of the sample before and after the first heating and cooling scans, passing from the fibrous structure to the melted one.

As expected, significantly lower crystallinity degree values were obtained due to the elimination of the fibrous structure, consequent to the first heating scan, in agreement with Liu, Yuan, and Bhattacharyya (2012).

3.4. Mechanical properties of PLA based mats

The stress–strain curves of the neat and hybrid PLA mats are compared in Fig. 4a.

In Table 3 the data of the uniaxial tensile tests, in terms of ultimate tensile stress (σ_{max}), yield stress (σ_s) and Young's modulus (E), are assembled. As it has been already pointed out elsewhere, the mechanical properties of electrospun mats are the result of a synergic combination of several factors as (Cacciotti, Calderone, & Bianco, 2013; Li, Cooper, Mauck, & Tuan, 2006): (i) intrinsic characteristics of the polymer which influence the fibers deformation mechanisms (whose increment causes a higher ultimate tensile stress);

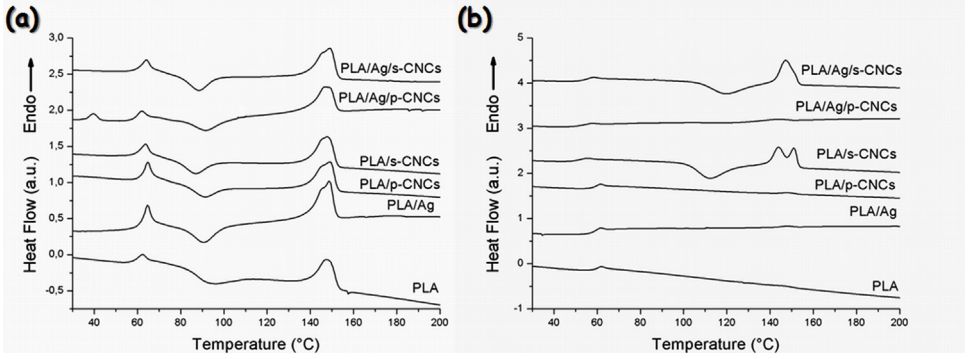

Fig. 3. First (a) and second (b) heating scan DSC curves of neat PLA and binary and ternary PLA based systems.

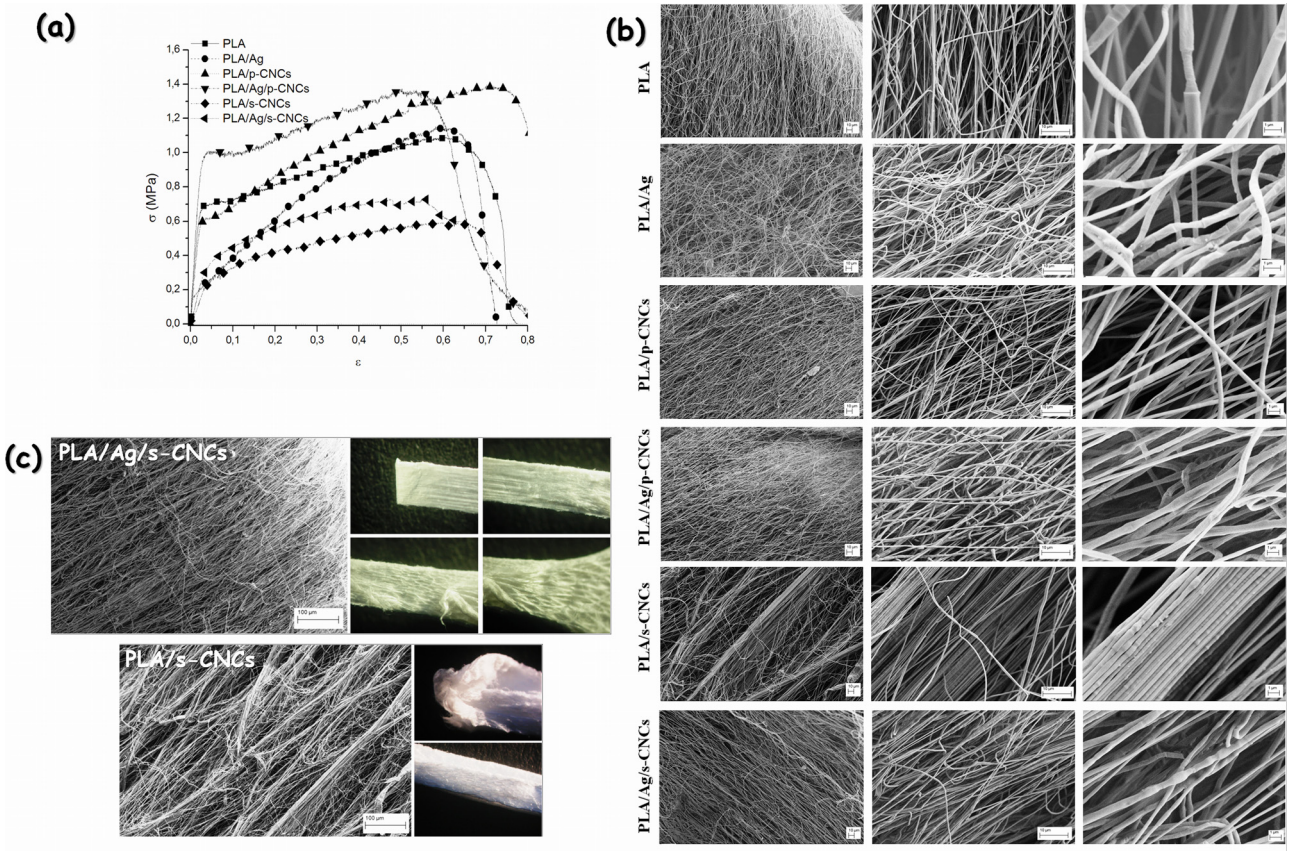

Fig. 4. (a) Stress–strain curves of neat PLA and binary and ternary PLA based systems; (b) SEM micrographs of stress–strained neat PLA and binary and ternary PLA based mats and (c) low magnification SEM micrographs and optical microscope pictures of stress–strained PLA/Ag/s-CNCs and PLA/s-CNCs mats.

(ii) fibers packing density, interaction and mechanical interlocking that increment the elastic modulus; (iii) fibers average diameter size (thinner fibers correspond to a higher packing density); (iv) presence of defects in the fibers.

The stiffness values of neat PLA and PLA/Ag produced mats (which measures the opposition to the alignment of the fibers in stress direction) were comparable (~27–28 MPa, Table 3), and it can be explained considering that these samples were composed of fibers of similar diameters and therefore presumably with the same interweave degree. Despite these systems presented similar ultimate tensile strength (Table 3), the yield stress of the binary PLA/Ag sample was poor ((0.16 ± 0.02) MPa, Table 3), showing weak mutual interaction among the single fibers (Li et al., 2006). Pristine CNCs containing mats showed a slight improvement of tensile strength and modulus in binary systems, which become much evident in PLA/Ag/p-CNCs ternary systems. These ternary mats presented increased yield and tensile strength, associable to the occurring of a synergic effect between the Ag and p-CNCs fillers. The SEM observation of the stress–strained mats revealed a fiber alignment in the direction of the stress and the presence of large necking areas, only interrupted by the presence of agglomerates, most probably silver clusters (Fig. 4b).

Both binary and ternary s-CNCs loaded mats showed a different and peculiar mechanical behavior with respect to the neat PLA and p-CNCs containing systems, presenting lower σ_{max} and E values (Table 3). These decreased mechanical properties can be considered the result of concomitant causes, since, as already underlined, in the case of electrospun systems, many factors can affect the mechanical performances, among which the chemical composition and the morphology play a critical role.

In particular, the surfactant in the s-CNCs loaded mats could act as plasticizer and lead to a decrement of the Young's modulus, as already observed in previous papers for s-CNCs loaded films (Fortunati, Armentano, Zhou, Puglia, et al., 2012) and corroborated

Table 3
Tensile modulus (E), ultimate tensile stress (σ_{max}) and yield stress (σ_s) from uniaxial tensile tests and storage modulus (E'), loss modulus (E'') and glass transition temperature (T_g) from DMTA analysis of neat and hybrid PLA based fibers (all values are expressed as mean values ± standard deviation (SD)).

Sample	Uniaxial tensile test			DMTA		
	E (MPa)	σ_s(MPa)	σ_{max}(MPa)	T_g(°C)	E' (MPa)	E'' (MPa)
PLA	28 ± 1	0.63 ± 0.01	1.10 ± 0.10	67.7 ± 0.9	28.6 ± 8.1	1.5 ± 0.5
PLA/Ag	27 ± 1	0.16 ± 0.02	1.15 ± 0.05	68.0 ± 0.7	37.7 ± 4.8	1.9 ± 0.1
PLA/p-CNCs	31 ± 2	0.60 ± 0.10	1.38 ± 0.10	68.1 ± 0.4	26.2 ± 9.1	1.2 ± 0.5
PLA/Ag/p-CNCs	39 ± 5	0.90 ± 0.10	1.40 ± 0.10	67.0 ± 0.1	44.8 ± 13.1	1.92 ± 0.8
PLA/s-CNCs	5.4 ± 0.5	0.21 ± 0.01	0.60 ± 0.10	65.8 ± 0.6	22.9 ± 7.0	2.3 ± 0.4
PLA/Ag/s-CNCs	9.8 ± 1.5	0.33 ± 0.05	0.73 ± 0.05	65.8 ± 0.5	21.7 ± 6.9	2.1 ± 0.6

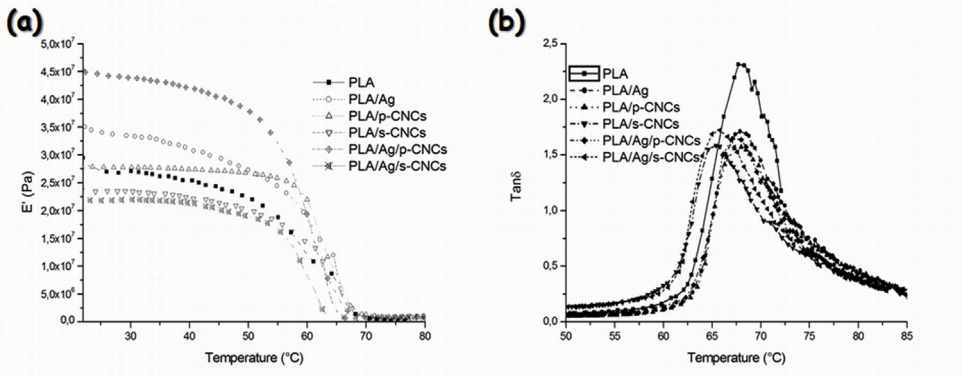

Fig. 5. Tan δ (a) and storage modulus (E') (b) curves of neat PLA and binary and ternary PLA based mats.

by the DSC results which evidenced a significant decrement of the T_g values during the second heating scan for the s-CNCs loaded mats (Table 2).

Furthermore, according to the authors, this decrement of the mechanical performances can be mainly imputed to the peculiar honeycomb morphology of the s-CNCs loaded mats. All samples, in fact, experienced a quick and evident delamination occurring at low loading conditions, between the layer with the honeycomb assembling of fibers and the below conventional mat layer, during the test, as evidenced in the related optical images of the fracture surface (Fig. 4c). Consequently this phenomenon caused detrimental effects on the mechanical properties since only a limited part of the mat sustained the load.

In agreement with the p-CNCs loaded mats, also in the case of the s-CNCs mats, an improvement of the mechanical data was observed for the ternary systems with respect to the binary ones, due to a synergic interaction between the s-CNCs and the Ag nanoparticles. From the reported optical images, it is possible to observe that the underneath fibrous layer was characterized by a marked fiber alignment in the load direction (Fig. 4c), behavior probably imputable to the co-presence of s-CNCs and Ag nanoparticles. In fact the PLA/s-CNCs mat presented lower fiber alignment degree (Fig. 4c), with the consequence that only the few fibers aligned in stress direction underwent necking and contributed to mat strength.

3.5. Viscoelastic properties of electrospun PLA based mats

The viscoelastic behavior of the nanocomposite fibrous mats was analyzed by means of the DMTA. In Table 3 the transition temperature (T_g) and the average values of storage dynamic modulus (E') and loss modulus (E'') at 25 °C are reported. This temperature was selected in order to investigate the thermo-mechanical properties for applications in the food packaging field, in order to identify systems with the optimal requirements for future developments as fillers in PLA matrix based composites.

The reported glass transition temperatures were evaluated as temperatures corresponding to the maximum value of the phase angle tangent (tan δ).

In the present study, it is important to note that for all samples the storage modulus (E') was about one order higher than the loss modulus (E''), thus evidencing an elastic behavior of the investigated mats (Table 3). In fact, the loss factor represents the proportion of the viscoelastic response of a material, corresponding tan $\delta = 0$ to a 100% elastic behavior, while tan $\delta = 1$ to a 50–50% elastic and viscoelastic behavior (François et al., 2010).

In Fig. 5a the tan δ curves of all samples are compared, revealing a remarkable decrement of the maximum peak intensity in the case of hybrid systems with respect to the neat PLA. This experimental evidence testified that well-dispersed nanofillers were able to delay the movements of the polymeric matrix segments during the glass transition.

Furthermore, the p-CNCs loaded mats presented neither significant shift nor broadening of the maximum peak, being characterized by T_g values comparable to the neat PLA (in the range 67–69 °C). On the other hand, the tan δ curves of s-CNCs loaded systems featured slightly lower T_g, indicating a better dispersion of the filler within the fibrous mat, and resulted broader than neat PLA one. This broadening corresponds to an increased temperature range for the glass transition, associated to an increment in the heterogeneity of the segmental mobilities and, thus, of the relaxation times distribution (Picciochi, Wang, Alves, & Mano, 2007). This experimental evidence suggested that the s-CNCs presence seemed to promote a different rearrangement of the polymeric chains. In fact the chain mobility of the polymer was enhanced, contributing to reduce the relaxation time needed for the glass transition and, therefore, less energy was needed for the transition from the glassy to the rubbery state (Picciochi, Wang, Alves, & Mano, 2007), supporting the recorded mechanical properties (Table 3).

It is important to highlight that the T_g values recorded by DMTA (Table 3) showed the same trend revealed for the T_g values acquired by DSC (Table 2), even if they were higher, as expected (Urayama, Ma, & Kimura, 2003; Wetton, 1993).

Comparing the storage dynamic modulus (E') curves and the DMTA data reported in Fig. 5b and Table 3, respectively, the PLA/p-CNCs showed values comparable to the neat PLA ones, whereas PLA/Ag and PLA/Ag/p-CNCs samples were characterized by higher E' values. This result can be ascribed to the inorganic filler which provides a higher rigidity, due to the restriction action of the Ag nanoparticles toward the polymeric chains mobility, to the reinforcement effect and to the higher modulus of the Ag nanoparticles.

In agreement with the tensile tests (Table 3), the s-CNCs loaded binary and ternary samples featured lower E' and E'' values, even if the registered decrement with respect to the neat PLA was remarkably inferior than that recorded by the tensile tests. Therefore, this result suggested that the morphological features played a pivotal role in determining the mechanical behavior.

4. Conclusions

Hybrid PLA based fibers, loaded with CNCs and silver nanoparticles, were successfully pursued by means of electrospinning technique, using 1 wt.% and 5 wt.% of Ag and CNCs, respectively. All the obtained mats were composed of smooth, randomly oriented, homogeneous, uniform and bead-free fibers whose average size ranged between (468 ± 111) nm and (551 ± 122) nm.

The addition of Ag and/or pristine p-CNCs fillers did not remarkably affect the fiber morphology and the average size dimension. On the other hand, more interestingly, the presence of surfactant

modified s-CNCs promoted the self-assembling of submicrometric (average diameter size 521 nm) fibers in bundles randomly organized in polygonal structures, such as pentagons and hexagons, resulting in a honeycomb-like network. This phenomenon is ascribable to the presence of residual charges on the collected nanofibers leading to the occurring of a self-organization and it was observed for PLA fibers for the first time.

The DSC and DMTA results suggested a good filler dispersion in the case of s-CNCs loaded samples, being characterized by lower cold crystallization and a shift of glass transition temperatures with respect to the neat PLA. Thus the s-CNCs acted as crystallization nuclei, thus promoting a different rearrangement of the polymeric chains.

Tensile tests and DMTA analysis revealed a slight improvement of the mechanical properties in the case of p-CNCs loaded fibers, particularly for the ternary systems, due to a synergic effect between the Ag and p-CNCs fillers. Both binary and ternary mats with s-CNCs fillers showed a peculiar mechanical behavior, characterized by lower Young's modulus and ultimate tensile stress. It is possible to hypothesize that such low mechanical performance can be ascribable to the plasticizer effect of the added surfactant and mainly to the occurring of a quick and evident delamination between the layer with the honeycomb assembling of fibers and the below conventional mat layer.

Thus, it is possible to modulate the morphological, thermal and mechanical properties of PLA fibers, properly selecting the fillers to use, in order to make them suitable for application in the food packaging sector. Future efforts will be devoted to employ the produced fibers as fillers in PLA matrix based composites, aimed at providing mechanical reinforcement, antimicrobial characteristics and improved barrier properties.

References

Ahirwal, D., Hébraud, A., Kádár, R., Wilhelm, M., & Schlatter, G. (2013). From self-assembly of electrospun nanofibers to 3D cm thick hierarchical foams. *Soft Matter*, *9*, 3164–3172.

Arecchi, A., Scampicchio, M., Drusch, S., & Mannino, S. (2010). Nanofibrous membrane based tyrosinase biosensor for the detection of phenolic compounds. *Analytica Chimica Acta*, *659*, 133–136.

Bianco, A., Bozzo, B. M., Del Gaudio, C., Cacciotti, I., Armentano, I., Dottori, M., et al. (2011). Poly(L-lactic acid)/calcium-deficient nanohydroxyapatite electrospun mats for murine bone marrow stem cell cultures. *Journal of Bioactive and Compatible Polymers*, *26*(3), 225–241.

Bianco, A., Di Federico, E., & Cacciotti, I. (2011). Electrospun poly(ε-caprolactone)-based composites using synthesized β-tricalcium phosphate. *Polymers for Advanced Technologies*, *22*, 1832–1841.

Bondeson, D., Mathew, A., & Oksman, K. (2006). Optimization of the isolation of nanocrystals from microcrystalline cellulose by acid hydrolysis. *Cellulose*, *13*(2), 171–180.

Bondeson, D., & Oksman, K. (2007). Dispersion and characteristics of surfactant modified cellulose whiskers nanocomposites. *Composite Interfaces*, *14*, 617–630.

Cacciotti, I., Calderone, M., & Bianco, A. (2013). Tailoring the properties of electrospun PHBV mats: Co-solution blending and selective removal of PEO. *European Polymer Journal*, http://dx.doi.org/10.1016/j.eurpolymj.2013.06.024

Cranston, E. D., & Gray, D. G. (2006). Morphological and optical characterization of polyelectrolyte multilayers incorporating nanocrystalline cellulose. *Biomacromolecules*, *7*, 2522–2530.

Deitzel, J. M., Kleinmeyer, J., Harris, D., & Tan, N. C. B. (2001). The effect of processing variables on the morphology of electrospun nanofibres and textiles. *Polymer*, *42*, 261–272.

Fortunati, E., Armentano, I., Zhou, Q., Iannoni, A., Saino, E., Visai, L., et al. (2012). Multifunctional bionanocomposite films of poly(lactic acid), cellulose nanocrystals and silver nanoparticles. *Carbohydrate Polymers*, *87*, 1596–1605.

Fortunati, E., Armentano, I., Zhou, Q., Puglia, D., Terenzi, A., Berglund, L. A., et al. (2012). Microstructure and nonisothermal cold crystallization of PLA composites based on silver nanoparticles and nanocrystalline cellulose. *Polymer Degradation and Stability*, *97*, 2027–2036.

Fortunati, E., Puglia, D., Santulli, C., Sarasini, F., & Kenny, J. M. (2012). Biodegradation of phormium tenax/poly(lactic acid) composites. *Journal of Applied Polymer Science*, *125*, E562–E572.

François, S., Sarra-Bournet, C., Jaffre, A., Chakfé, N., Durand, B., & Laroche, G. (2010). Characterization of an air-spun poly(L-lactic acid) nanofiber mesh. *Journal of Biomedical Materials Research B: Applied Biomaterials*, *93*(2), 531–543.

Frenot, A., & Chronakis, I. S. (2003). Polymer nanofibers assembled by electrospinning. *Current Opinion in Colloid and Interface Science*, *8*, 64–75.

Galina Rodionova, G., Lenes, M., Eriksen, Ø., & Gregersen, Ø. (2011). Surface chemical modification of microfibrillated cellulose: Improvement of barrier properties for packaging applications. *Cellulose*, *18*, 127–134.

He, Y., Fan, Z., Wei, J., & Li, S. (2006). Morphology and melt crystallization of poly(L-lactide) obtained by ring opening polymerization of L-lactide with zinc catalyst. *Polymer Engineering and Science*, *46*, 1583–1589.

Heux, L., Chauve, G., & Bonini, C. (2000). Nonflocculating and chiral-nematic self-ordering of cellulose microcrystals suspensions in nonpolar solvents. *Langmuir*, *16*(21), 8210–8212.

Huang, Z.-M., Zhang, Y.-Z., Kotaki, M., & Ramakrishna, S. (2003). A review on polymer nanofibers by electrospinning and their applications in nanocomposites. *Composites Science and Technology*, *63*, 2223–2253.

Huda, M. S., Drzal, T., Misra, M., & Mohanty, A. K. (2006). Wood-fiber-reinforced poly(lactic acid) composites: Evaluation of the physicomechanical and morphological properties. *Journal of Applied Polymer Science*, *102*(5), 4856–4869.

Huda, M. S., Drzal, L. T., Mohanty, A. K., & Misra, M. (2007). The effect of silane treated- and untreated-talc on the mechanical and physico-mechanical properties of poly(lactic acid)/newspaper fibers/talc hybrid composites. *Composites Part B: Engineering*, *38*(3), 367–379.

Jiang, H., Hu, Y., Li, Y., Zhao, P., Zhu, K., & Chen, W. (2005). A facile technique to prepare biodegradable coaxial electrospun nanofibers for controlled release of bioactive agents. *Journal of Controlled Release*, *108*, 237–243.

Kijchavengkul, T., Auras, R., Rubino, M., Ngouajio, M., & Fernandez, R. T. (2006). Development of an automatic laboratory-scale respirometric system to measure polymer biodegradability. *Polymer Testing*, *25*, 1006–1016.

Kriegel, C., Arrechi, A., Kit, K., McClements, D. J., & Weiss, J. (2008). Fabrication, functionalization, and application of electrospun biopolymer nanofibers. *Critical Reviews in Food Science and Nutrition*, *48*, 775–797.

Lagaron, J. M., & Lopez-Rubio, A. (2011). Nanotechnology for bioplastics: Opportunities, challenges and strategies. *Trends in Food Science and Technology*, *22*, 611–617.

Lamastra, F. R., Puglia, D., Monti, M., Vella, A., Peponi, L., Kenny, J. M., et al. (2012). Poly(ε-caprolactone) reinforced with fibres of poly(methyl methacrylate) loaded with multiwall carbon nanotubes or graphene nanoplatelets. *Chemical Engineering Journal*, *195/196*, 140–148.

Li, W.-J., Cooper, J. A., Jr., Mauck, R. L., & Tuan, R. S. (2006). Fabrication and characterization of six electrospun poly(α-hydroxy ester)-based fibrous scaffolds for tissue engineering applications. *Acta Biomaterialia*, *2*(4), 377–385.

Lim, S. K., Son, T. W., Lee, D. W., Park, B. K., & Cho, K. M. (2001). Novel regenerated cellulose fibers from rice straw. *Journal of Applied Polymer Science*, *82*, 1705–1708.

Liu, D., Yuan, X., & Bhattacharyya, D. (2012). The effects of cellulose nanowhiskers on electrospun poly(lactic acid) nanofibres. *Journal of Materials Science*, *47*, 3159–3165.

Morozov, V. N., & Vsevolodov, N. N. (2007). Electrospray-neutralization method for manufacturing free and supported nanomats. *Advanced Materials*, *19*, 4381–4386.

Ochi, S. (2008). Mechanical properties of kenaf fibers and kenaf/PLA composites. *Mechanics of Materials*, *40*, 446–452.

Oksman, K., Mathew, A. P., Bondeson, D., & Kvien, I. (2006). Manufacturing process of cellulose whiskers/polylactic acid nanocomposites. *Composites Science and Technology*, *66*, 2776–2784.

Petersen, K., Nielsen, P. V., & Olsen, M. B. (2001). Physical and mechanical properties of biobased materials. *Starch*, *53*(8), 356–361.

Picciochi, R., Wang, Y., Alves, N. M., & Mano, J. F. (2007). Glass transition of semicrystalline PLLA with different morphologies as studied by dynamic mechanical analysis. *Colloid and Polymer Science*, *285*(5), 575–580.

Qi, H., Hu, P., Xu, J., & Wang, A. (2006). Encapsulation of drug reservoirs in fiber by emulsion electrospinning. Morphology characterization and preliminary release assessment. *Biomacromolecules*, *7*, 2327–2330.

Ramakrishna, S., Fujihara, K., Teo, W. E., Lim, T. C., & Ma, Z. (2005). *An introduction to electrospinning and nanofibers*. Singapore: World Scientific Publishing.

Ramakrishna, S., Jose, R., Archana, P. S., Nair, A. S., Balamurugan, R., Venugopal, J., et al. (2010). Science and engineering of electrospun nanofibers for advances in clean energy, water filtration, and regenerative medicine. *Journal of Materials Science*, *45*, 6283–6312.

Riga, A., Zhang, J., & Collis, J. (2004). Characterization of drawn and undrawn poly-L-lactide films by differential scanning calorimetry. *Journal of Thermal Analysis and Calorimetry*, *75*, 257–268.

Sanchez-Garcia, M. D., Lopez-Rubio, A., & Lagaron, J. M. (2010). Natural micro and nanobiocomposites with enhanced barrier properties and novel functionalities for food biopackaging applications. *Trends in Food Science and Technology*, *21*, 528–536.

Sarasua, J. R., López Arraiza, A., Balerdi, P., & Maiza, I. (2005). Crystallization and thermal behaviour of optically pure polylactides and their blends. *Journal of Materials Science*, *40*(8), 1855–1862.

Shi, Q. F., Mou, H. Y., Gao, L., Yang, J., & Guo, W. H. (2010). Double-melting behavior of bamboo fiber/talc/poly(lactic acid) composites. *Journal of Polymers and the Environment*, *18*, 567–575.

Shi, Q., Zhou, C., Yue, Y., Guo, W., Wu, Y., & Wu, Q. (2012). Mechanical properties and in vitro degradation of electrospun bio-nanocomposite mats from PLA and cellulose nanocrystals. *Carbohydrate Polymers*, *90*, 301–308.

Sim, K. J., & Han, S. O. (2010). Dynamic mechanical and thermal properties of red algae fiber reinforced poly(lactic acid) biocomposites. *Macromolecular Research*, *18*, 489–495.

Siracusa, V., Rocculi, P., Romani, S., & Dalla Rosa, M. (2008). Biodegradable polymers for food packaging: A review. *Trends in Food Science and Technology*, *19*, 634–643.

Suksut, B., & Deeprasertkul, C. (2011). Effect of nucleating agents on physical properties of poly(lactic acid) and its blend with natural rubber. *Journal of Polymers and the Environment*, *19*(1), 288–296.

Thandavamoorthy, S., Gopinath, N., & Ramkumar, S. S. (2006). Self-assembled honeycomb polyurethane nanofibers. *Journal of Applied Polymer Science*, *101*, 3121–3124.

Urayama, H., Ma, C., & Kimura, Y. (2003). Mechanical and thermal properties of poly(L-lactide) incorporating various inorganic fillers with particle and whisker shapes. *Macromolecular Materials and Engineering*, *288*, 562–568.

Weiss, J., Takhistov, P., & McClements, D. J. (2006). Functional materials in food nanotechnology. *Journal of Food Science*, *71*, R107–R116.

Wetton, R. E. (1993). In B. J. Hunt, & M. I. James (Eds.), *Polymer characterisation* (p. 178). London: Blackie.

Xiang, C. H., Joo, Y. L., & Frey, M. W. (2009). Nanocomposite fibers electrospun from poly(lactic acid)/cellulose nanocrystals. *Journal of Biobased Materials and Bioenergy*, *3*, 147–155.

Yan, G., Yu, J., Qiu, Y., Yi, X., Lu, J., Zhou, X., et al. (2011). Self-assembly of electrospun polymer nanofibers: A general phenomenon generating honeycomb-patterned nanofibrous structures. *Langmuir*, *27*, 4285–4289.

Wu, D., Wu, L., Wu, L., Xu, B. I. N., Zhang, Y., & Zhang, M. (2007). Non-isothermal cold crystallization behavior and kinetics of polylactide/clay nanocomposites. *Journal of Polymer Science Part B: Polymer Physics*, *45*, 1100–1113.

Zong, X., Kim, K., Fang, D., Ran, S., Hsiao, B. S., & Chu, B. (2002). Structure and process relationship of electrospun bioabsorbable nanofiber membranes. *Polymer*, *43*, 4403–4412.